

# Wavelet Analysis of Permanent Magnet Synchronous Machine Flux Density Harmonic Content With Different Pole Number Designs

**O. A. Mohammed, FIEEE, N. Y. Abed, S. Ganu, and S. Liu, Member IEEE**  
**Energy Systems Laboratory, Department of Electrical and Computer Engineering**  
**Florida International University**  
**Miami, FL, 33174 USA**

**Abstract**— This paper utilizes the wavelet packet transform to study the effects of decreasing the number of slots per pole per phase on the harmonic behavior of the working flux density in the air gap. A surface mounted PM motor is used as an example. The original design contains 6 PM poles and 36 stator slots with three phase winding embedded. The rotor is redesigned to have 4, 8, and 12 poles mounted on the same rotor iron surface and the winding is rearranged to form 4, 8, and 12 stator poles respectively with the original 36 slots stator. The air gap flux density waveform along a round path close to teeth surface is obtained from the FE solutions. The harmonic behavior of air gap flux is studied with a wavelet packet transform. It is found that an increase the number of poles causes an increase in the harmonic content of the air-gap flux density and the accompanying effects on the proper operation other components connected to external circuits.

**Keywords:** FEM, harmonics, wavelet packet transform, THBD

## I. INTRODUCTION

Conventional analytical design and analysis methods of AC machines follow the assumption of having sinusoidal flux waveform in the air gap. An increase in the number of poles can be utilized for increasing the machine power density or for satisfying the lower speed demands at some application fields. This means in turn reduces the number of slots per pole per phase.

Decreasing the slot number per rotor pole per phase may lead to harmonic behavior increase in the air gap flux waveform. Harmonics increase can be the source of a variety of undesirable effects in the energy system. For example, harmonics can cause signal interference, over voltages, and circuit breaker failure, as well as equipment overheating, malfunction, and failure. Harmonics can cause excessive heating in system components, resulting in shortened life or failure. Rotor heating and pulsating output torque caused by harmonics can result in excessive motor heating and inefficiency. In other words, the harmonic increase will affect both the machine performance and the machine control system performance. Also, it will have negative effect on the other NEPS components and operation.

Wavelet transform proves to have some advantages when compared to the classical FFT-based algorithms. One of the basic assumptions of the FFT, the periodicity of the signal, is not required and erroneous results are avoided. The wavelet methods solve this problem by decomposing the measurement signal into a family of time finite signals through a filter-bank resulting in multi-scale wavelet decomposition. Harmonics of the fundamental frequency, sub-harmonics and inter-harmonics are considered, disregarding the length of their occurrence in time.

With the help of FE analysis and Wavelet packet, the effects of the decrease the number of slots per pole per phase on the harmonic behavior of the air gap flux density waveform is investigated.

In order to rebuild various pole designs, such as the 4-pole, 8-pole and 12-pole based on the original 6-pole machine, the windings need to be rearranged to carry the three-phase current in the slots. The FE computation is performed on the various designs to obtain the filed distribution and the flux density waveform in the air gap. Wavelet and wavelet packets are introduced and utilized to analyze the flux density waveforms in the air gap. The effect of the decreasing the number of slots per pole per phase on the working flux is then discussed.

# Report Documentation Page

Form Approved  
OMB No. 0704-0188

Public reporting burden for the collection of information is estimated to average 1 hour per response, including the time for reviewing instructions, searching existing data sources, gathering and maintaining the data needed, and completing and reviewing the collection of information. Send comments regarding this burden estimate or any other aspect of this collection of information, including suggestions for reducing this burden, to Washington Headquarters Services, Directorate for Information Operations and Reports, 1215 Jefferson Davis Highway, Suite 1204, Arlington VA 22202-4302. Respondents should be aware that notwithstanding any other provision of law, no person shall be subject to a penalty for failing to comply with a collection of information if it does not display a currently valid OMB control number.

1. REPORT DATE <b>23 APR 2004</b>		2. REPORT TYPE <b>N/A</b>		3. DATES COVERED <b>-</b>	
4. TITLE AND SUBTITLE <b>Wavelet Analysis of Permanent Magnet Synchronous Machine Flux Density Harmonic Content With Different Pole Number Designs</b>				5a. CONTRACT NUMBER	
				5b. GRANT NUMBER	
				5c. PROGRAM ELEMENT NUMBER	
6. AUTHOR(S)				5d. PROJECT NUMBER	
				5e. TASK NUMBER	
				5f. WORK UNIT NUMBER	
7. PERFORMING ORGANIZATION NAME(S) AND ADDRESS(ES) <b>Energy Systems Laboratory, Department of Electrical and Computer Engineering Florida International University Miami, FL, 33174 USA</b>				8. PERFORMING ORGANIZATION REPORT NUMBER	
9. SPONSORING/MONITORING AGENCY NAME(S) AND ADDRESS(ES)				10. SPONSOR/MONITOR'S ACRONYM(S)	
				11. SPONSOR/MONITOR'S REPORT NUMBER(S)	
12. DISTRIBUTION/AVAILABILITY STATEMENT <b>Approved for public release, distribution unlimited</b>					
13. SUPPLEMENTARY NOTES <b>See also ADM001763, Annual Review of Progress in Applied Computational Electromagnetics (20th) Held in Syracuse, NY on 19-23 April 2004., The original document contains color images.</b>					
14. ABSTRACT					
15. SUBJECT TERMS					
16. SECURITY CLASSIFICATION OF:			17. LIMITATION OF ABSTRACT	18. NUMBER OF PAGES	19a. NAME OF RESPONSIBLE PERSON
a. REPORT <b>unclassified</b>	b. ABSTRACT <b>unclassified</b>	c. THIS PAGE <b>unclassified</b>			

II. MOTOR TOPOLOGIES FOR FIELD ANALYSIS

A. Original design and redesigns

The structure of the original surface mounted PM synchronous motor has 6 poles on the rotor iron and 36 slots in the stator iron. The winding is double layer and excited with 3 phase supply. Slots per pole per phase (spp) are  $2(36/3*6)$ . The winding arrangement for complete machine is shown in Fig.1(a). The magnets are radially magnetized. Their operating point is  $B_r = 1.08$  Tesla and  $\mu_r = 1.07$ . The angular magnet pole width is 50 mechanical degree. Nonlinear BH curves are used for both stator and rotor iron. In order to form different number of poles, the stator winding needs to be rearranged so as to form same number of poles on stator as that of rotor. Winding arrangement for different number of poles is also shown in the Fig.1 (b),(c),(d). Depending on the number of poles, spp will change. As the number of poles goes on increasing, each phase will occupy less number of slots.

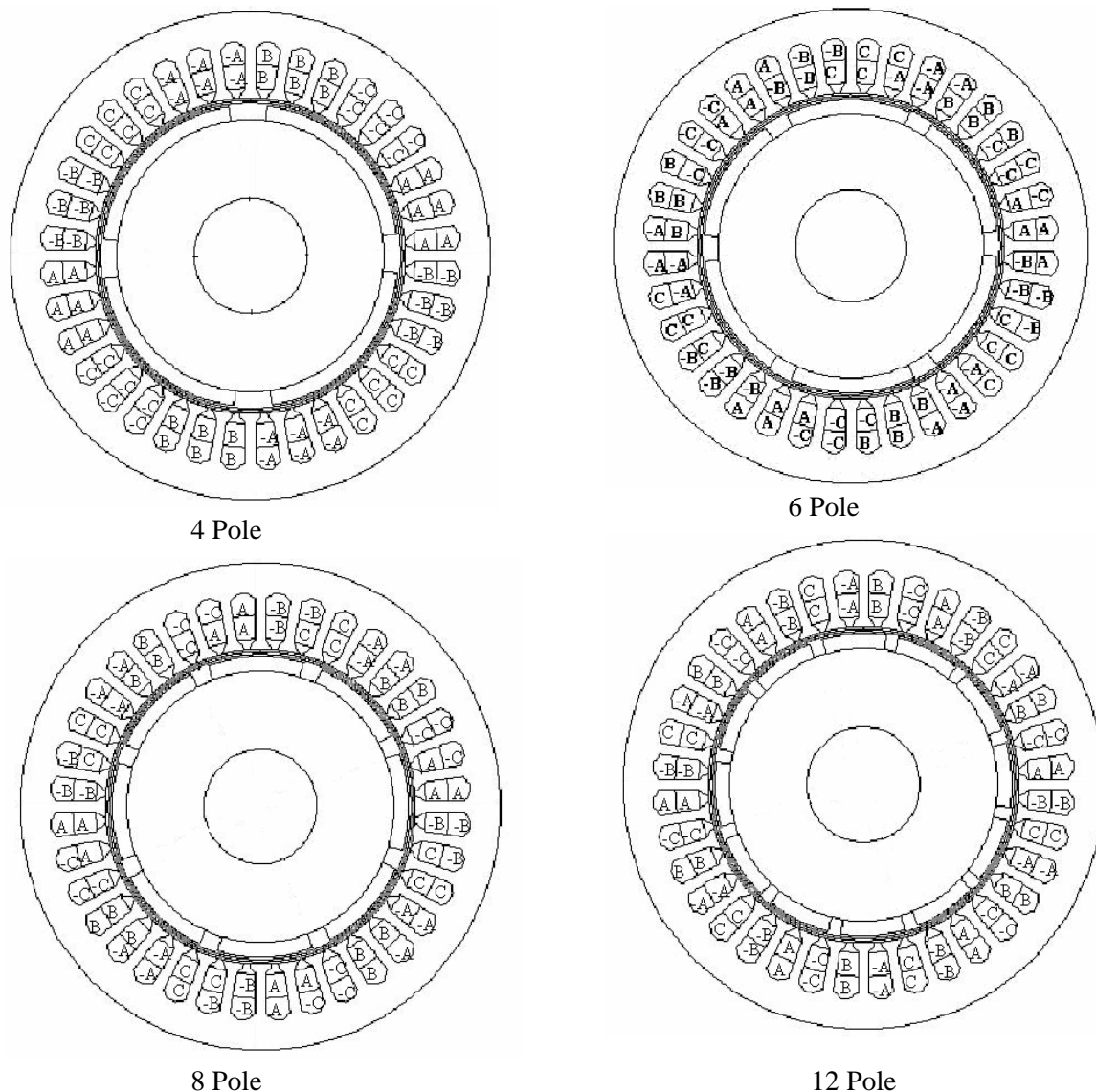


Fig. 1 Winding arrangement and pole design variation

The redesigned rotors are shown in Fig.1. The angular magnetic pole width is kept constant for all the pole variations. The air gap between permanent magnets is adjusted accordingly to form a whole circle. The

dimensions of the stator yoke, rotor yoke and stator teeth in all the topologies are kept unchanged. All radial and axial dimensions for motor are same.

Obviously, iron part in the motor having higher number of poles will be operating at higher flux density level and goes towards saturation. Saturation is one of the important factors causing harmonic increase in the air gap waveforms along with slotting effects.

### B. FEM analysis and considerations

Following formulation is used for solving the transient magnetic solution

$$\sigma \frac{\partial \bar{A}}{\partial t} + \nabla \times (\nu \nabla \times \bar{A}) = \sigma \nabla V + \nabla \times \bar{H}_c \quad (1)$$

$\bar{H}_c$  = coercive magnetic field of the magnet

$V$  = Electric potential

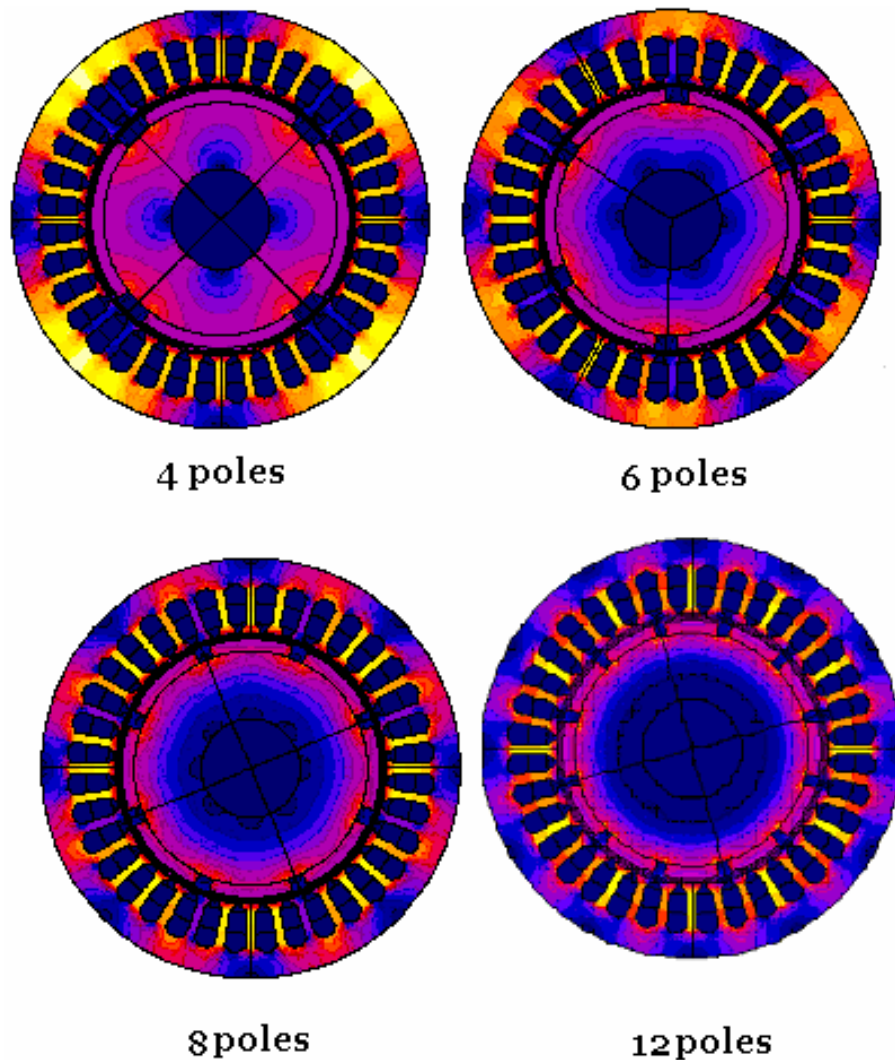


Fig. 2 Surface flux density distribution for different pole number designs

Nonlinear transient FE analysis was performed for the field calculation. Parameters used for the transient solution include time step of 0.3125ms corresponding to 3.75 degrees of rotor movement, 48 steps over 180 degrees of electrical cycle. Moving air gap feature is utilized for the transient operation. The air gap is divided into 3 layers, one belonging to stator, one to the rotor and middle one which actually causes the rotor to move with respect to stator without changing the mesh.

Considering motor periodicities, only quarter geometry is modeled for 4, 8, 12 poles while for 6 poles one third geometry is modeled. Results shown in here are at 0.015sec time instant. Fig. 2 shows the flux density distribution profiles. Fig. 3 shows the air gap flux density waveform along the center locus of the air gap at the same time instance.

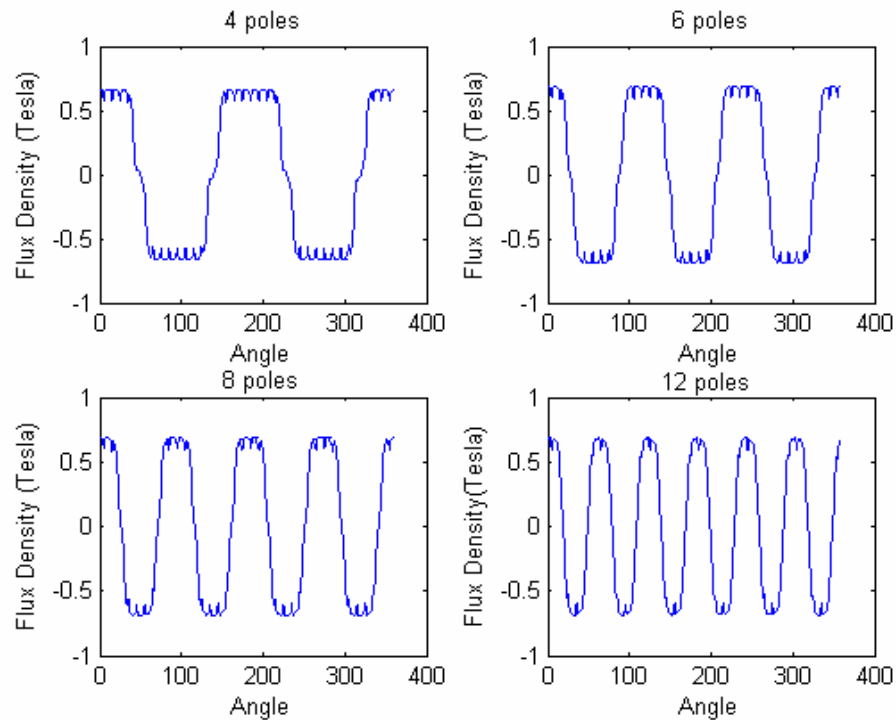


Fig. 3 Flux density along the locus at the center of air gap

### III. WAVELET THEORY

#### A. Introduction

As in Fourier analysis, the wavelet transform consists in decomposing a given function onto a set of “building blocks”. However, as opposed to the Fourier transformation (FT) in which the “building blocks” are the well-known complex exponentials, the wavelet transform uses the dilated and translated version of a “mother wavelet” which has convenient properties according to time/frequency localization. Unlike FT which gives a global presentation of the signal, Wavelet transform provides a local representation (in both time and frequency) of a signal; therefore it’s suitable for analyzing a signal where Time/frequency resolution is needed.

#### B. Multiresolution analysis

A multiresolution analysis of  $L^2(\mathbb{R})$  is defined as a sequence of closed subspaces  $V_j$  of  $L^2(\mathbb{R})$ ,  $j \in \mathbb{Z}$ , with the following properties [1-5]:

- $V_j \subset V_{j+1}$
- $v(x) \in V_j \Leftrightarrow v(2x) \in V_{j+1}$
- $v(x) \in V_0 \Leftrightarrow v(x+1) \in V_0$
- $\bigcup_{j=-\infty}^{+\infty} V_j$  is dense in  $L^2(\mathbb{R})$  and  $\bigcap_{j=-\infty}^{+\infty} V_j = \{0\}$
- A scaling function  $\varphi \in V_0$ , with a non-vanishing integral, exists such that the collection  $\{\varphi\{x \leftrightarrow l\} | l \in \mathbb{Z}\}$ , is a Riesz basis of  $V_0$ .

A signal can be successively approximated by wavelets with different scales (multiresolution decomposition). Each step of the decomposition of signal corresponds to a certain resolution. The decomposition process can be iterated, with successive approximations being decomposed in turn, so that one signal is broken down into many lower-resolution components. This is called the wavelet decomposition tree. For n-level decomposition, there are n+1 possible ways to decompose or encode the signal.

The *wavelet packet transform (WPT)* method is a generalization of wavelet decomposition. In wavelet packet analysis, the details as well as the approximations can be split. This yields more than  $2^{2^{n-1}}$  different ways to encode the signal. Wavelet packet decomposition is depicted in Figure 4 (a)

Let  $\phi(t)$  and  $\psi(t)$  be the scaling function and the corresponding mother wavelet function in the conventional DWT and define  $\psi^0(t) = \phi(t)$ , and  $\psi^1(t) = \psi(t)$ ,

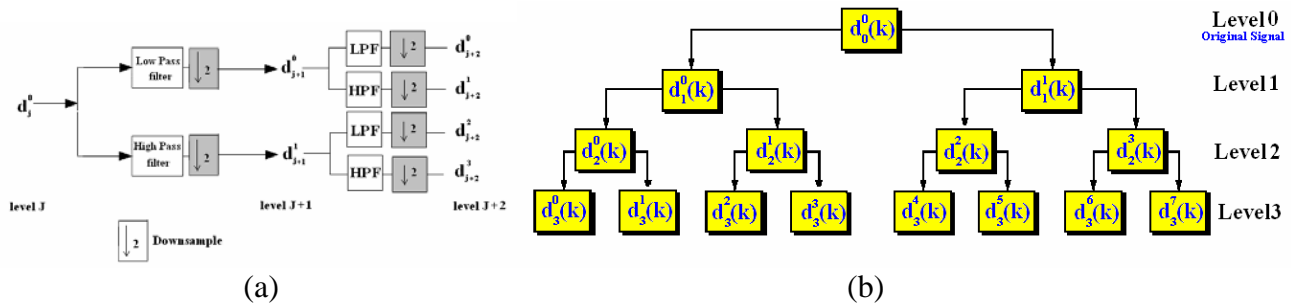


Fig. 4 (a) Wavelet packet decomposition with successive filtering and down sampling.  
 (b) Three level wavelet packet decomposition

For  $2^N$  sampled waveform the wavelet transform coefficients (WTCs) of a given function B(t) at the J level and kth point can be evaluated obtained by convolving the sequence  $d_{j-1}^i(k)$  with a low pass filter (LPF), and then downsampling by a factor of two. In the same manner, coefficients (WTCs) of a given function B(t) at the (2i+1)th node can be evaluated obtained by convolving the sequence  $d_{j-1}^i(k)$  with a High pass filter (LPF), and then downsampling by a factor of two. Number of bands at jth level is  $2^j$ . Mathematically, the (WTCs) can be written as:

$$d_j^{2i}(k) = \int B(t)\psi_{j,k}^{2i}(t)dt = \sum_n h(n)d_{j-1}^i(2k-n)$$

$$d_j^{2i+1}(k) = \int B(t)\psi_{j,k}^{2i+1}(t)dt = \sum_n g(n)d_{j-1}^i(2k-n)$$
(2)

Where

$$\psi_{j,k}^{2i}(t) = \frac{1}{\sqrt{2^j}}\psi^{2i}\left(\frac{2^j k-t}{2^j}\right) = \sum_n h(n)\psi_{j-1,2k-n}^i(t)$$

$$\psi_{j,k}^{2i+1}(t) = \frac{1}{\sqrt{2^j}}\psi^{2i+1}\left(\frac{2^j k-t}{2^j}\right) = \sum_n g(n)\psi_{j-1,2k-n}^i(t)$$

They are the wavelet basis function where  $j=0,1,\dots,N$  and  $i = 0,1,\dots,2^{j-1} - 1$

Since the wavelet basis are orthogonal, the following properties should be fulfilled:

$$\begin{aligned} \int \psi_{j,k}^p(t) dt &= 0 & p &= \text{integer} \\ \int \psi_{j,k}^p(t) \psi_{j,k}^q(t) &= \begin{cases} 1 & p=q \\ 0 & p \neq q \end{cases} \\ \int (\phi_{j,k}(t))^2 &= 1 \\ \int \phi_{j,k}(t) \psi_{j,k}^p(t) &= 0 & p &\neq 0 \end{aligned} \quad (3)$$

A three level wavelet packet decomposition tree is shown in Fig.4b. Each tree represents the signal decomposition as depicted in Fig. 4a.

#### IV. WAVELET REPRESENTATION OF RMS AND TOTAL HARMONIC DISTORTION

In the wavelet theory, any waveform can be expressed in term of it's weighted sums of wavelet basis function [1,2,4,6-12], hence B(t) can be expressed as:

$$B(t) = \sum_{i=0}^{2^{j-1}-1} \sum_{k=0}^{2^{N-j}-1} d_j^{2i}(k) \psi_{j,k}^{2i}(t) + \sum_{i=0}^{2^{j-1}-1} \sum_{k=0}^{2^{N-j}-1} d_j^{2i+1}(k) \psi_{j,k}^{2i+1}(t) = \sum_{k=0}^{2^{N-j}-1} d_j^0(k) \phi_{j,k}(t) + \sum_{i=1}^{2^{j-1}-1} \sum_{k=0}^{2^{N-j}-1} d_j^i(k) \psi_{j,k}^i(t) \quad (4)$$

Where  $d_j^0(k)$  is the scaling function coefficients .

RMS of a waveform with period T can be expressed in terms of wavelet at a certain level J as follows:

$$\begin{aligned} \int B(t)^2 dt &= \int \left[ \sum_{k=0}^{2^{N-j}-1} d_j^0(k) \phi_{j,k}(t) + \sum_{i=1}^{2^{j-1}-1} \sum_{k=0}^{2^{N-j}-1} d_j^i(k) \psi_{j,k}^i(t) \right]^2 dt = \int \left[ \sum_{k=0}^{2^{N-j}-1} d_j^0(k) \phi_{j,k}(t) \right]^2 dt + \int \left[ \sum_{i=1}^{2^{j-1}-1} \sum_{k=0}^{2^{N-j}-1} d_j^i(k) \psi_{j,k}^i(t) \right]^2 dt \\ &\quad + 2 \int \left( \sum_{i=1}^{2^{j-1}-1} \sum_{k=0}^{2^{N-j}-1} d_j^0(k) d_j^i(k) \phi_{j,k}(t) \psi_{j,k}^i(t) \right) \\ &= \int \sum_{k=0}^{2^{N-j}-1} (d_j^0(k))^2 \int [\phi_{j,k}(t)]^2 dt + \sum_{i=1}^{2^{j-1}-1} \sum_{k=0}^{2^{N-j}-1} (d_j^i(k))^2 \int [\psi_{j,k}^i(t)]^2 dt + 2 \left( \sum_{i=1}^{2^{j-1}-1} \sum_{k=0}^{2^{N-j}-1} d_j^0(k) d_j^i(k) \int \phi_{j,k}(t) \psi_{j,k}^i(t) dt \right) \end{aligned} \quad (5)$$

Using the wavelet orthogonality property, Equation 5 becomes:

$$\int B(t)^2 dt = \sum_{i=0}^{2^j-1} \sum_{k=0}^{2^{N-j}-1} (d_j^i(k))^2 \quad (6)$$

The RMS of the flux waveform can now found by divide by the wave period T and take the root square of equation 6.

$$B_{rms} = \sqrt{\frac{1}{T} \int_0^T B(t)^2 dt} = \sqrt{\frac{1}{2^N} \sum_{n=0}^{2^N-1} B(n)^2} = \sqrt{\frac{1}{2^N} \sum_{n=0}^{2^j-1} \sum_{k=0}^{2^{N-j}-1} (d_j^i(k))^2} = \sqrt{\sum_{n=0}^{2^j-1} (B_j^i)^2} \quad (7)$$

$$B_j^i = \sqrt{\frac{1}{2^N} \sum_{k=0}^{2^{N-j}-1} (d_j^i(k))^2} \quad (8)$$

Where,  $B_j^i$  is the RMS value of frequency band at node  $i$ . The Total Harmonic band distortion (THBD) is defined by the ratio of the RMS value of the harmonic bands at  $i > 0$  (i.e. excluding the lowest band) to the RMS value of the distorted waveform. The THBD for the flux density waveform is given by the following relation:

$$\text{THBD} = \frac{1}{B_{rms}} \sqrt{\sum_{i=1}^{2^j-1} (B_j^i)^2} \quad (9)$$

## V. RESULTS

This technique has been applied to the flux density in the middle of the air gap generated from the finite element model. The files were then used as input to our Wavelet packets module to extract the different harmonic bands of the flux density waveform.

A five level decomposition was selected to perform our study. This will decompose the signal into 32 frequency band ( $2^5$ ). The first eight are enough to evaluate the harmonic behaviors.

Table 1 show the analysis result of the flux waveform for the first 4 frequency band for 4, 6, 8 and 12 poles PM-machines respectively. From the analysis it's clear that there is increase in harmonics contents within the flux density with the number of poles increase. Fig. 5 shows the relation between number of poles increase and the total band harmonic distortion. There is a small increase in the THBD from 4 to 6 poles machine. On the other hand bigger increase is noticed between 6 and 8 poles, 6 and 12 poles, and 8 and 12 poles respectively.

From these results it's obvious that there is an increase in the harmonics content with in the flux density waveform with number of poles increase.

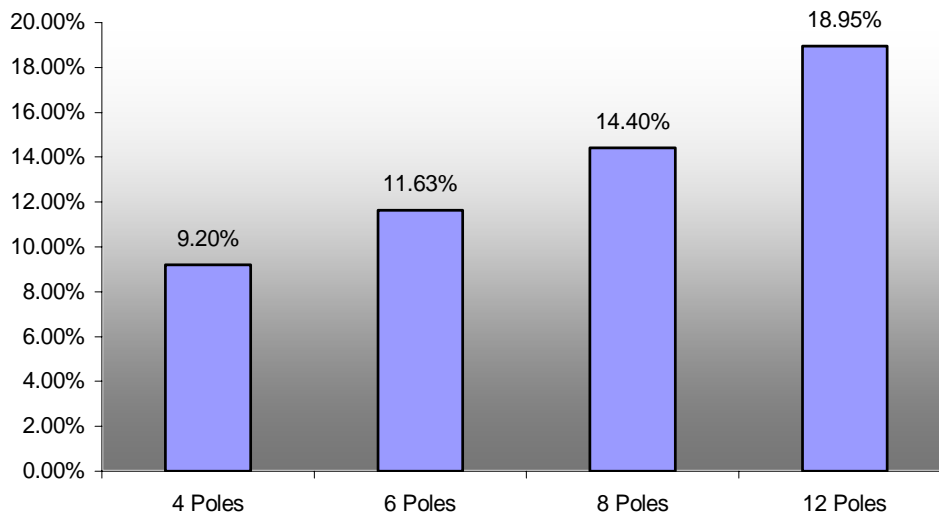


Fig.5 THBD change with number of poles change

## VI. CONCLUSION

FEM simulation presents an effective method for studying the influence of number of slots per pole per phase decrease on the harmonic content of the working flux density. Finite element analysis allows us to determine the flux density in the air gap.

A wavelet packets technique was used to evaluate the harmonic behavior for different number of poles. The property of WPT analysis shows an ability to quantify different types of disturbances. It also shows high ability of wavelets to extract the different harmonic components disregarding the length of their occurrence in time. The harmonic contents tend to increase with number of poles increase. The results of are very useful in the design and development of both the motor and drive's diagnosis systems.

As a future study we will consider the effects of PM Pole structure and the rotor surface on the working flux, which is also one of the important factors affecting the harmonic behavior of working flux.

Table 1 Total Harmonic distortion for different number of poles

	THD %	RMS	Band 0 0-75Hz	Band 1 75-150Hz	Band 2 150-225Hz	Band 3 225-300Hz	Band 4 300-375Hz
4 poles	9.2	0.5737	0.5713	0.0432	0.0212	0.0145	0.0103
6 poles	11.63	0.5913	0.5873	0.0576	0.0280	0.0153	0.0137
8 poles	14.4	0.5824	0.5766	0.0695	0.0331	0.0144	0.0168
12 poles	18.95	0.5600	0.5498	0.0907	0.0446	0.0166	0.0219

## VII. ACKNOWLEDGEMENT

Part of this work is supported by a grant from the Office of Naval Research.

## VIII. REFERENCES

- [1] G. Wornell, "Signal Processing with Fractals: A wavelet-Based Approach," Prentice Hall, 1996.
- [2] Gerald Kaiser, "A Friendly Guide to Wavelets" Springer Verlag, 1994
- [3] V. K. Madisetti, and D. B. Williams, "Digital Signal Processing Handbook," CRC Press, 1999.
- [4] W.Yoon, and M. Devancy, "Power Measurement using the wavelet Transform," IEEE Transactions on Instrumentation and Measurements, Vol. 47, NO.5, OCT 1998.
- [5] J. C. Goswami, and A .K .Chen," Fundamentals of wavelets", John Wiley, 1999.
- [6] E. Hamid, Z. Kawasaki, H. Yoshida, and H. Doi, "Wavelet Analysis of Voltage Disturbances for Power Quality Applications," IEE of Japan. Vol.122, No.2, February 2002.
- [7] P.L. Mao, and R.K. Aggarwal, "A novel approach to the classification of the transient phenomena in power transformers using combined wavelet transform and neural network", IEEE Transactions on Power Delivery, Vol. 16, No. 4, Oct. 2001.
- [8] L. Angrisani,; P. Daponte,; M. D'Apuzzo,; and A. Testa," A measurement method based on the wavelet transform for power quality analysis," IEEE Transactions on Power Delivery , Vol.13, No. 4 , Oct. 1998
- [9] W. Press et al., Numerical Recipes in Fortran, Cambridge University Press, New York, 1992
- [10] A. W. Galli "Analysis of Electrical Transients In Power Systems Via A Novel Wavelet Recursion Method," Purdue University, 1997
- [11] Fan Wang, "On Power Quality and Protection," Thesis, Chalmers University of Technology, 2000.
- [12] D. Elliott, "Handbook of Digital Signal Processing: Engineering Applications," Academic Press, INC, 1987.